Proceedings of 20th International Congress on Acoustics, ICA 2010

23-27 August 2010, Sydney, Australia

FDTD techniques applied to acoustic propagation in vegetable tissue: the Elastodynamic Behavior of the Orange Fruit

Noé Jiménez, Rubén Picó, Javier Redondo, Francisco Camarena, Bernardino Roig

(1) Instituto para la Gestión Integrada de Zonas Costeras. Universidad Politécnica de Valencia. 46730 Grao de Gandia, Spain.

PACS: 43.35.Pt; 43.80.Ev; 02.70.Bf

ABSTRACT

The plant tissues, in particular the orange's skin, are essentially aqueous-filled structures of varying density and elasticity composed by fat and acids substances, as well as areas of intercellular air. In recent years many techniques have been developed for ultrasonic characterization of fruit and vegetables in postharvest processes. All have found common macroscopic acoustic parameters: a slow propagation speed and a large absorption. It is intended therefore to obtain a prediction model of ultrasounds propagation in this viscoelastic heterogeneous media by FDTD (Finite Difference Time Domain) techniques. Thus, this paper presents a time domain numerical model for simulating acoustic propagation in plant tissue. This model correctly describes the special characteristics of wave propagation experimentally detected in these biological tissues, emphasizing the need for elastic frequency dependent characteristics: a frequency dependent elasticity modulus. These simulation results will be compared with measures obtained from an experimental device to validate the numerical model. Thus, the validation of a model of mechanical wave propagation in heterogeneous media has a great interest because it will deepen the understanding and development of new techniques for characterization of complex materials, providing tools for predicting propagation processes in this kind of media.

INTRODUCTION

There are many techniques for monitoring the quality of horticultural products in post-harvest processes and each of them is based on the measurement of a physical-chemical parameter in search of finding a correlation with a physiological index that correctly describes the physiological, biochemical and structure of the fruit. Nowadays, there are numerous methods of fruit quality monitoring, but most of them require a destructive test, so they cannot be applied to all fruits and vegetables in a production line [1].

In recent years, many articles have been published describing trials to develop non-destructive techniques for the generation and detection of ultrasonic waves in plant tissues as the proposed for avocado and mango [2], for apples [3, 4], for potatoes [5, 6], in carrots [7], or in oranges [8, 9]. Due to the special acoustic characteristics of these media, the experimental set-up described in these papers has a very narrow bandwidth and a low ultrasonic resonant frequency that varies between 37 and 100 kHz. At higher frequencys the ultrasonic wave are strongly attenuated [10]. The results of these tests provide two important conclusions about the propagation of acoustic waves in plant tissues. First, low propagation velocities detected in these kinds of media, below 200 m / s for surface measurements. The second one is a high wave attenuation, which varies between 1 and 7dB/mm depending on the type of tissue [10].

There are many simulation studys of acoustics waves in vegetable tissues on frequency domain. In this way, have been developed finite element numerical simulations to determine acoustics resonances in pears [12] in melons [13, 14], and in apples [15]. These studies numerically estimate the resonance frequencies of the fruit in order to determine fruit firmness using the relationship proposed by J. R. Cooke [11] on spherical fruits.

Other finite element simulations have also described the elastic behavior of plant tissues on a microscopic scale, as in [16] where a model of cell blocks for simulations of stress-strain is implemented; or in [17], where the mechanical modeling of epidermal cells of onion is considered.

In this work, a finite difference time domain method (FDTD) is applied in order to simulate the ultrasonic wave propagation through the orange fruit tissue (*Citrus Sinensis (L.) Osbeck*).

DYNAMIC ELASTIC PARAMETERS OF THE ORANGE FRUIT

The orange tissue can be divided from an elastodynamic point of view in three different layers. The outermost part of the fruit peel is the orange pigmented shell namely flavedo where there are many volatile oil glands in pits. Inward this, there is a porous white color layer, the albedo. Finally, the waterlike tissue core of the orange is composed with fluid-

filled vesicles called carpels containing the orange juice and seeds.

Due to the complexity of the inner structure of vegetal tissues, different approaches can be considered to model the propagation of elastic waves through the orange tissue. The elevated content of water in fruits suggests that it may be appropriate to apply a fluid model for wave propagation studies. Besides, as transverse waves are not allowed to propagate in Newtonian fluids, it is necessary to incorporate the shear elasticity in the model. In order to do that, the well known model for linear elastic solid is proposed: that is a solid for which the strain is fully determined by the stress. As the cell structure of the orange is very small compared to the typical wavelength of ultrasounds on these media, it can be assumed that the tissue can be homogenized and can be fully described by its linear elastic properties. The model describes wave propagation in a linear elastic solid, which is isotropic and without damping. Later, viscous losses are added to the model.

The elastic properties of these heterogeneous media had been studied for many authors with stress-strain experimental techniques [19, 20]. Some of these studies conclude that the orange peel shows a viscoelastic behavior, so that the elasticity proprieties may vary with the frequency. In fact, the ultrasound speed of the longitudinal, shear and Rayleigh surface waves calculated from these stress-strain elastic constants is approximately of 20-30 m/s, too low compared with measured values with the ultrasonic studies [9].

To explain these higher values of propagation speed obtained with ultrasonics techniques, we suppose that the elastic constants at higher frequencies are higher than the ones measured with stress-strain mechanical techniques (at very low frequencies or constant stress). In order to take into account this elastic behavior we use higher elasticity values than the cited in bibliography. Because the fruit peel is a waterlike tissue we suppose that the pressure wave speed c_p is similar than in water. In addition, the Poisson's ratio of these tissues is in the range 0.49-0.5 [21], so the measured Rayleigh wave speed is about $c_R \approx 0.95 c_s$ [22]. Finally, the elasticity values of the orange peel are such that holds:

$$\lambda + 2\mu = \rho c_{p,water}^2 \tag{1}$$

$$\mu = \rho\left(0.95 c_{R,measured}\right)^2 \tag{2}$$

where λ and μ are the elastic constants (Lamé's constants) and ρ is the density of the solid, c_p is the longitudinal propagation speed of the waterlike media (1500m/s) and c_R is the experimental ultrasonic measured Rayleigh wave speed. The empirically deduced elastic parameters are listed in table 1.

Table 1. Empirically deduced media parameters

Parameter	Air	Flavedo	Albedo	Inner core
Density, ρ (kg/m³)	1.21	903	820	978
Lame's 1º λ (MPa)	-0.142	$1{,}95 \cdot 10^3$	$0{,}62 \cdot 10^3$	$-2.2 \cdot 10^3$
Lame's 2º, μ (MPa)	0	36	10,8	0
Young Modulus, E (MPa)	-	107,3	22,2	-
Poisson's Ratio, v	-	0,491	0. 25	-

For the fruit's fluid inner core, the value of the Bulk modulus is similar than water, neglecting for this media the action of fluid-shear stresses of this biological structure. The values for the Bulk density are measured with the Archimedes principle. The values for the resistance coefficients (η_P, η_S; see equations 5-7) for the longitudinal and transverse waves are derived from the empirically measured attenuation coefficient.

SURFACE WAVE FDTD SIMULATION

Equations of the model

The main equations of the problem can be deduced from the second Newton's law and the Hooke's law [23], in velocity-stress formulation can be written as:

$$\frac{\partial \boldsymbol{\tau}}{\partial t} = \lambda \bar{\mathbf{I}}\left(\nabla \cdot \boldsymbol{v}\right) + \mu\left(\nabla \boldsymbol{v} + \boldsymbol{v}\nabla\right) \tag{3}$$

$$\rho \frac{\partial \boldsymbol{v}}{\partial t} = \nabla \cdot \boldsymbol{\tau} \tag{4}$$

where $\boldsymbol{\tau}$ is the stress tensor, and $\boldsymbol{v}$ is the first time derivative of the strain. This model accounts for the propagation of two kind of volumetric waves. The first is a longitudinal wave or compression waves (*p-wave*), analogue to the waves present in fluids. They have the same direction of oscillation along their direction of travel, which means that the oscillation of the medium (particle) is in the same direction or opposite direction as the motion of the wave. The speed c_P of this wave can be calculated as $c_P = ((\lambda+2\mu)/\rho)^{0.5}$.The second is a transverse wave or shear wave (s-wave). In this case, oscillations are perpendicular to the direction of energy transfer. The speed c_S of this wave in a solid is $c_S = (2\mu/\rho)^{0.5}$. It is important to remark that other kind of waves can propagate because of the interface of two elastic solids. Hence, a Rayleigh wave can propagate as a surface wave between both two elastic media. Particles disturbed by a Rayleigh wave oscillate with an elliptical polarization in the sagittal plane respect to the propagation direction of the wave.

In order to incorporate the attenuation of the ultrasonic wave, a damping term is added, which on a 3D cartesian coordinate system leads to a 9 equations set:

$$\rho \frac{\partial v_\xi}{\partial t} = \frac{\partial \tau_{\xi\xi}}{\partial \xi} + \frac{\partial \tau_{\psi\psi}}{\partial \psi} + \frac{\partial \tau_{\xi\zeta}}{\partial \zeta} \tag{5}$$

$$\frac{\partial \tau_{\xi\xi}}{\partial t} + \eta_P \tau_{\xi\xi} = \left(\lambda + 2\mu\right)\frac{\partial v_\xi}{\partial \xi} + \lambda \frac{\partial v_\psi}{\partial \psi} + \lambda \frac{\partial v_\zeta}{\partial \zeta} \tag{6}$$

$$\frac{\partial \tau_{\xi\psi}}{\partial t} + \eta_S \tau_{\xi\psi} = \mu \frac{\partial v_\xi}{\partial \psi} + \lambda \frac{\partial v_\psi}{\partial \xi} \tag{7}$$

where (ξ, ψ, ζ = *x*, *y*, *z*) and η_P, η_S are the resistance coefficients related to the attenuation coefficient of the longitudinal and shear wave respectively [24].

Numerical Scheme

An explicit finite difference method was used for the elastodynamic behavior simulation of the orange fruit. Thus, the linear solid equations are discretized using central-difference approximations to the space and time partial derivatives, which lead to a spatially staggered discretization of the velocity, normal and shear stress fields, and a temporal staggered discretization of particle velocity vector and stress tensor (Figure 1). In addition, with this numerical method it is possible to implement fluid heterogeneities inside the elastic solid media making the λ and μ values in this region to be $-k$ and 0 respectively; where k is the Bulk modulus of the fluid media.

For implement the numerical model of the orange, the domain has been divided into three concentric spherical shells.

The surrounding outer layer of the orange domain is air. The first layer is the fruit external orange shell, the flavedo, of 2 mm thick, 50 mm curvature radius and whose properties are listed in Table 1. Inland is the albedo layer, 3 mm thick and 48 mm curvature radius. The inner fluid core of the fruit is a sphere with 45 mm of curvature radius.

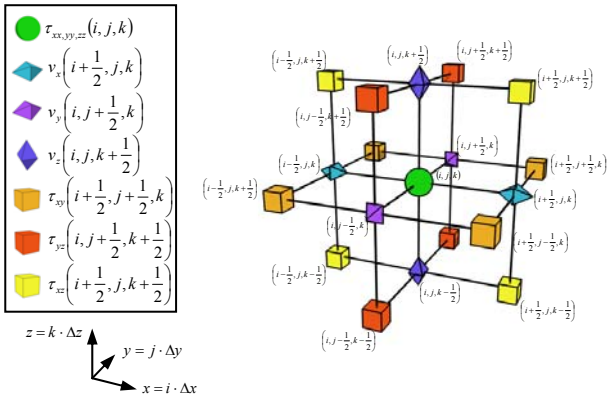


Figure 1. Spatial discretization for velocity and stress fields

This space is discretized by a cubic grid with the side length of $3{,}025 \cdot 10^{-5}$ m, which leads to 10.8 elements per wavelength for transversal waves, and 142.1 n/λ for longitudinal waves at a frequency of 40 kHz. The temporal step of the algorithm was chosen to preserve a maximum courant number of 0.8 over all subdomains, and the stability conditions at media interface must be satisfied [25]. Due to the high computational cost of algorithm simulates only a sector of the total orange's domain, hence a 12 elements perfect matched layer (PML) was used as absorbing boundaries. The PML implementation was based on the time-dependent form of the stretched coordinate formulation [26], with a quadratic profile and values of $\Omega_{max}=5.02 \cdot 10^{-5}$ *rad/s* and $\alpha_{max}=2$. The excitation signal was a negative normalized second derivative of a Gaussian function, also known as a "Ricker wavelet", and the central frequency was 40 kHz.

EXPERIMENTAL SET-UP

In order to validate the numerical model for the propagation of the elastic waves through orange tissue, a no destructive test was performed on a seven set of Navel cultivar sweet orange (*Citrus Sinensis (L.) Osb*). The two transducers used were sandwich type with a mechanical focuser to maximize the power transfer to the plant tissue in emission-reception configuration. In the nondestructive test configuration, transducers are placed on the surface without damaging the fruit. Thus, varying the separation between transducers can measure the received signal and calculate some acoustic properties of the medium. The tests were performed during two months after the harvest and the set of oranges were storage in a dry room at 20º C. The results shows that the propagation speed on the surface of the orange does not exceed 280 m/s at any time, increasing function of time since 120 m/s to final mean values of 220 m/s. In the other hand, the high attenuation coefficient of the media varies from 1dB/mm to 3dB/mm.

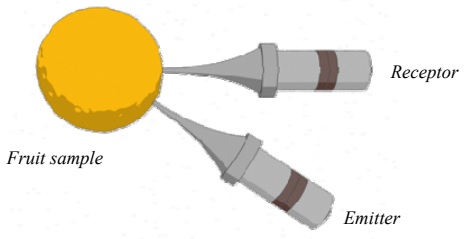


Figure 2. Experiemenal set-up for ultrasonic measure

RESULTS

Several measurements over radially distributed points at he surface of the fruit in order to calculate the propagation speed. Thus, the configuration of this model is very similar to experimental set-up of the tests. Figure 3 represents a time-space plot showing the recorded temporal signals versus the distance to excitation source. A linear fit by least squares over the traces of equal wave phase in time and space allows the estimatation the propagation speed of the ultrasonic wave. The fit shows that two different waves are detected on the surface of the orange model without damping: the steeper slope corresponds to the longitudinal wave propagation speed while the less steep slope corresponds to the surface wave.

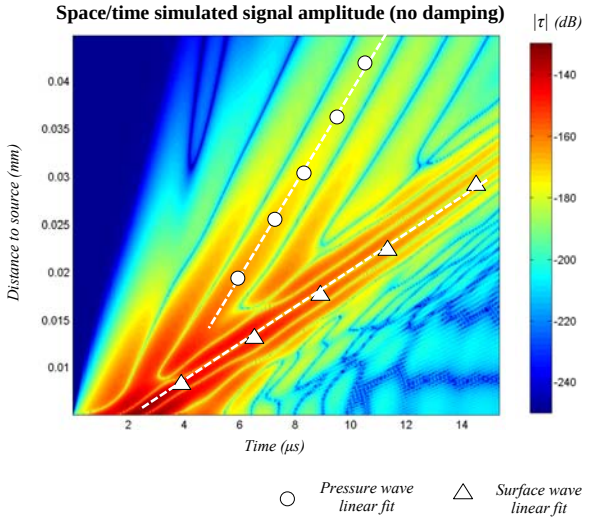


Figure 3. Space-time diagram for the fruit model without damping.

With the aim of taking into account the high absorption of the vegetable tissue, a second model was simulated setting the resistance coefficients to the empirically measured wave attenuation of 3dB/mm as proposed in literature [9]. By a similar linear fit by least squares the propagation wave speed was estimated. Results show that only a low propagation speed wave is present due the high damping on the recorded signals. The fit for the model with damping was x=183,978t-0,0043 (m); so the value of the propagation speed is similar to the theoretical predicted for a Rayleigh surface wave. Comparing with the theoretical Rayleigh speed $c_{R,\ theoretical}$ = 197.42 m/s calculated for a Poisson ratio of 0.491 with that obtained numerically ($c_{R,\ numeric}$ = 183.97 m/s) yields an error of 6.8%. Yet we must bear in mind that the theoretical speed may vary if the surface geometry is curvilinear and whether there are heterogeneities [27]. Because the amplitude of the traces of the velocity of longitudinal wave propagation is very low it was decided to make several adjustments to reduce uncertainty. Thus, as a result of these adjustments a propagation velocity c_P = 1357.40 m/s is obtained, representing an error of 9.5% compared with the theoretical longitudinal velocity in a homogeneous medium without curvilinear geometry.

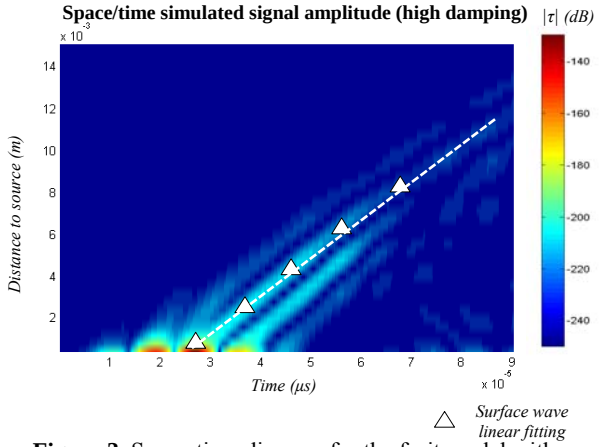


Figure 3. Space-time diagram for the fruit model with 3dB/mm viscous losses.

However, a deeper analysis is needed to study if the motion of the orange tissue is a pure shear wave or another surface wave as Rayleigh or lamb waves. We this aim, the velocity of particle is represented as a function of depth and normalizing the depth respect to the wavelength, which is around 5 mm on the tissue surface. We can see that in spite of the heterogeneity of the environment and the curvilinear geometry of the tissue structure, we can appreciate different features specific of surface waves.

Figure 4 shows that the particle velocity components are spatially offset, so that the longitudinal component is highest when the horizontal component is minimal. On the other hand, the wave is attenuated as a function of depth, and even the curvilinear geometry of our problem, cannot penetrate to a distance greater than λ. Finally, below a depth of about 0.2 λ the velocity components are reversed which means that the elliptical motion described by the particles also do that: on the surface the particle motion describe ellipses pass backward in the sagittal plane, at a depth of 0.2 λ the particle motion have a minimum in all components and below the particle elliptical motion turn in the opposite direction.

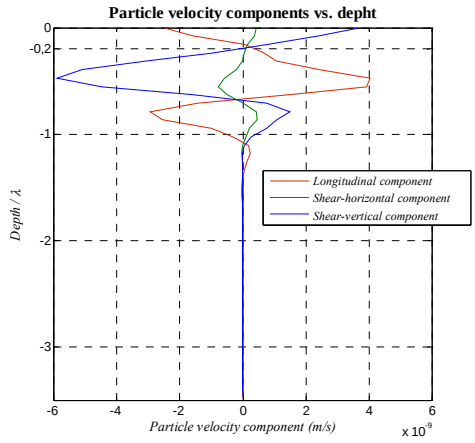


Figure 4. Particle velocity components recorded at maximum signal amplitude time versus orange's skin depth.

CONCLUSION

The study and understanding of the nature of elastic waves in plant tissues can be approached by finite difference methods. In this work, cartesian 3D-FDTD techniques have been applied to solve an elastodynamic problem. The complex heterogeneous media of an orange fruit can be approximated by a linear elastic model. The values of the computed propagation surface wave speed are very close to the values of the experimentally measured waves, and with this model the longitudinal wave is strongly attenuated on the surface. On other hand, with these values of propagation speed one can calculate the linear elastic parameters, which are well correlated of the post-harvest quality of fruit.

ACKNOWLEDGEMENTS

This work has been supported financially by Programa de Apoyo a la Investigación y Desarrollo of the Universidad Politécnica de Valencia (PAID-05-09) (002-618) y (PAID-06-08) de la Universidad Politécnica de Valencia, Spain.

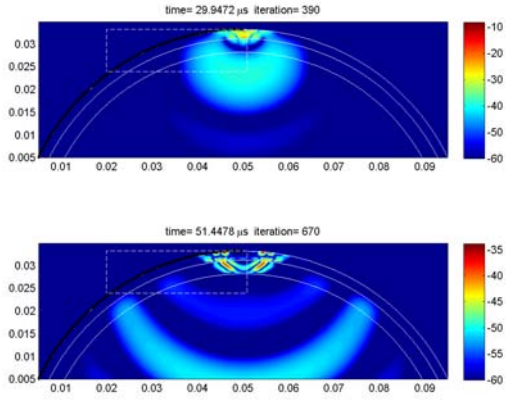
REFERENCES

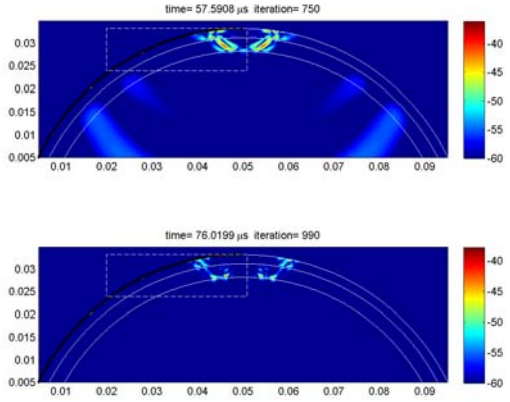
1 Ladaniya Milind S. *Citrus Fruit - Biology, technology and evaluation*. Academic Press, Elsevier, 2008.
2 Mizrach A. "Determination of avocado and mango fruit properties by ultrasonic technique". *Ultrasonics*. 38 (1-8):717 (2000)
3 Bechar A. "Determination of mealiness in apples using ultrasonic measurements." *Biosystems engineering*. 91(3):329 (2005)
4 Kim K. B. "Determination of apple firmness by ultrasonic measurement." XVIII Imeko World Congress, Metrology for a Sustainable Development. Rio de Janeiro, Brazil (2006).
5 Cheng Y. y Haugh C.G. "Detecting Hollow Heart in Potatoes Using Ultrasound." *Transactions of the ASAE*. 37(1):217-222 (1994)
6 Jivanuwong Solos. "Nondestructive detection of hollow heart in potatoes using ultrasonics". PDThesis – Virginia Polytechnic Institute and State University (1998).
7 Nielsen M. "Low frequency ultrasonics for texture measurements in cooked carrots (Daucus carota L.)" *Journal of food science*. 62(6):1167 (1997)
8 Camarena F. y Martínez-Mora J.A. "Potential of ultrasound to evaluate turgidity and hydration of the orange peel" *Journal of food engineering*. 75(4):503 (2006)
9 Camarena F., Martínez-Mora J.A. y Ardid M. "Ultrasonic study of the complete dehydration process of orange peel" *Postharvest biology and technology*. 43(1):115 (2007)
10 Mizrach A. "Ultrasonic technology for quality evaluation of fresh fruit and vegetables in pre-and postharvest processes". *Postharvest biology and technology*. 48:315–330 (2008)
11 Cooke J.R. y Rand R.H. "A mathematical study of resonance in intact fruits and vegetables using 3 media elastic sphere model" *J. Agric. Eng. Res.* 18:141–157 (1973)
12 Dewulf W. "Determining the firmness of a pear using finite element modal analysis" *Journal of agricultural engineering research*. 74(3):217 (1999)
13 Jancsok P. T. et al. "Investigation of the effect of shape on the acoustic response of conference pears by finite element modelling". *Postharvest biology and technology*. 23(1):1 (2001)
14 Nourain J. et al. "Firmness evaluation of melon using its vibration characteristic and finite element analysis." *Journal of Zhejiang University*. 6B(6):483-490 (2005)
15 Kim G. W. "Determination of the viscoelastic properties of apple flesh under quasi-static compression based on finite element method optimization." *Food Science and Technology Research*. 14(3):221 (2008)

16 Wu N; Pitts M.J. "Development and validation of a finite element model of an apple fruit cell". *Postharvest Biology and Technology*. 16:1-8 (1999)
17 Loodts J., et. al. "Micromechanics: Simulating the elastic behavior of onion epidermis tissue." *Journal of texture studies*. 37:16 (2006)
18 Mebatsion H. K. "Modelling fruit (micro) structures, why and how?" *Trends in food science & technology*. 19(2):59 (2008)
19 Fidelibus M., Teixeira A. A. y Davies F. S. "Mechanical propieties of orange peel and fruit treated pre-harvest with gibberellic acid" *Transactions of the ASAE*. 45(4):1057-1062 (2002)
20 Singh Krishna K. y B. Sreenivasula "Post-harvest physico-mechanical properties of orange peel and fruit." *Journal of Food Engineering*. 73:112–120 (2006)
21 Goss S.A., Johnston R.L. y Shnol S.E. "Comprehensive compilation of empirical ultrasonic properties of mammalian tissues" *J. Acoust. Soc. Am*. 64(2):423–457 (1978)
22 Malischewsky P.G. "Comparison of approximated solutions for the phase velocity of Rayleigh waves" *Nanotechnology*. 16:995–996 (2005)
23 Auld B.A. *Acoustic Fields and Elastic Waves in Solids*. (Wiley, New York, 1973) Vol. I and II.
24 Hosokawa A. "Development of a Numerical Cancellous Bone Model for Finite-Difference Time-Domain Simulations of Ultrasound Propagation" *EEE transactions on ultrasonics, ferroelectrics, and frequency control*. 55(6):1219 (2008)
25 Schröder Christoph T.; Scott Waymond R. "On the Stability of the FDTD Algorithm for Elastic Media at a Material Interface." *IEEE Transactions on Geoscience and Remote Sensing*. 40(2):474 (2002)
26 Chew W. C. y Liu Q. "Perfectly matched layers for elastodynamics: a new absorbing boundary condition". *J. Comput. Acoust*. 4(4):341-359 (1996)
27 Jin F. "Basic properties of Rayleigh surface wave propagation along curved surfaces". *International journal of engineering science*. 43.3-4:250 (2005)

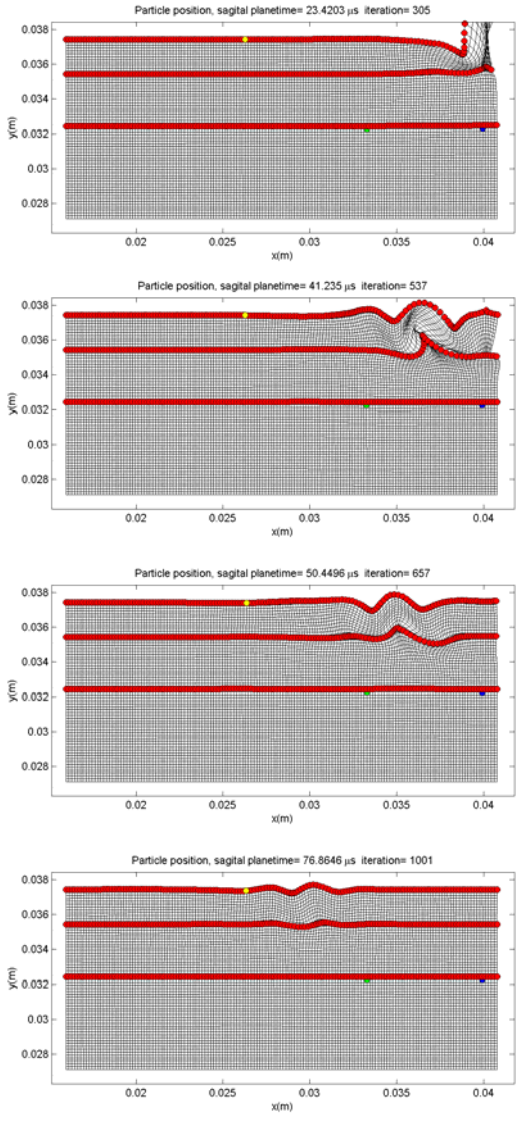
APPENDIX A

Snapshots of the the normal strain modulus is plotted illustrating the elastodynamic behaviour of the modeled orange fruit. The figures shows the three wave motion predicted: the large wavelength pressure wave, the shear wave and the Raileigh surface wave.





On another secuence, snapshots of the particle position can be obtained from the discrete integral of the particle velocity vector and adding the initial balance position. The amplitude of the motion in the pictures below is magnified in a factor of 10^3. In the secuence one can appreciatte how the longitudinal wave is strongly attenuated and only the Raileigh wave can travel along the surface in the model with viscous losses.



APPENDIX B

Splitted equations for implement the perfect matched layers (PML) on a 3D cartesian linear elastic solid with viscous losses. The subscripts denote the physical component of the

velocity-stress fields while the superscripts mean the splitted sub-component. This set of 24 equations is discretised through finite diferences leading an explicit method to solve the velocity-strain fields in time domain. Thus, for the 9 splitted components of particle velocity:

$$\rho\left(\alpha_x \frac{\partial v_x^x}{\partial t} + \Omega_x v_x^x\right) = \frac{\partial \tau_{xx}}{\partial x} \tag{8}$$

$$\rho\left(\alpha_y \frac{\partial v_x^y}{\partial t} + \Omega_y v_x^y\right) = \frac{\partial \tau_{xy}}{\partial y} \tag{9}$$

$$\rho\left(\alpha_z \frac{\partial v_x^z}{\partial t} + \Omega_z v_x^z\right) = \frac{\partial \tau_{zx}}{\partial z} \tag{10}$$

$$\rho\left(\alpha_x \frac{\partial v_y^x}{\partial t} + \Omega_x v_y^x\right) = \frac{\partial \tau_{xy}}{\partial x} \tag{11}$$

$$\rho\left(\alpha_y \frac{\partial v_y^y}{\partial t} + \Omega_y v_y^y\right) = \frac{\partial \tau_{yy}}{\partial y} \tag{12}$$

$$\rho\left(\alpha_z \frac{\partial v_y^z}{\partial t} + \Omega_z v_y^z\right) = \frac{\partial \tau_{yz}}{\partial z} \tag{13}$$

$$\rho\left(\alpha_x \frac{\partial v_z^x}{\partial t} + \Omega_x v_z^x\right) = \frac{\partial \tau_{zx}}{\partial x} \tag{14}$$

$$\rho\left(\alpha_y \frac{\partial v_z^y}{\partial t} + \Omega_y v_z^y\right) = \frac{\partial \tau_{yz}}{\partial y} \tag{15}$$

$$\rho\left(\alpha_z \frac{\partial v_z^z}{\partial t} + \Omega_z v_z^z\right) = \frac{\partial \tau_{zz}}{\partial z} \tag{16}$$

The 9 splitted set of the normal strain:

$$\alpha_x \frac{\partial \tau_{xx}^x}{\partial t} + (\Omega_x + \eta_P)\tau_{xx}^x = (\lambda + 2\mu)\frac{\partial v_x}{\partial x} \tag{17}$$

$$\alpha_y \frac{\partial \tau_{xx}^y}{\partial t} + (\Omega_y + \eta_P)\tau_{xx}^y = \lambda \frac{\partial v_y}{\partial y} \tag{18}$$

$$\alpha_z \frac{\partial \tau_{xx}^z}{\partial t} + (\Omega_z + \eta_P)\tau_{xx}^z = \lambda \frac{\partial v_z}{\partial z} \tag{19}$$

$$\alpha_x \frac{\partial \tau_{yy}^x}{\partial t} + (\Omega_x + \eta_P)\tau_{yy}^x = \lambda \frac{\partial v_x}{\partial x} \tag{20}$$

$$\alpha_y \frac{\partial \tau_{yy}^y}{\partial t} + (\Omega_y + \eta_P)\tau_{yy}^y = (\lambda + 2\mu)\frac{\partial v_y}{\partial y} \tag{21}$$

$$\alpha_z \frac{\partial \tau_{yy}^z}{\partial t} + (\Omega_z + \eta_P)\tau_{yy}^z = \lambda \frac{\partial v_z}{\partial z} \tag{22}$$

$$\alpha_x \frac{\partial \tau_{zz}^x}{\partial t} + (\Omega_x + \eta_P)\tau_{zz}^x = \lambda \frac{\partial v_x}{\partial x} \tag{23}$$

$$\alpha_y \frac{\partial \tau_{zz}^y}{\partial t} + (\Omega_y + \eta_P)\tau_{zz}^y = \lambda \frac{\partial v_y}{\partial y} \tag{24}$$

$$\alpha_z \frac{\partial \tau_{zz}^z}{\partial t} + (\Omega_z + \eta_P)\tau_{zz}^z = (\lambda + 2\mu)\frac{\partial v_z}{\partial z} \tag{25}$$

The 6 splitted set for the shear strain:

$$\alpha_x \frac{\partial \tau_{xy}^x}{\partial t} + (\Omega_x + \eta_S)\tau_{xy}^x = \mu \frac{\partial v_y}{\partial x} \tag{26}$$

$$\alpha_y \frac{\partial \tau_{xy}^y}{\partial t} + (\Omega_y + \eta_S)\tau_{xy}^y = \mu \frac{\partial v_x}{\partial y} \tag{27}$$

$$\alpha_y \frac{\partial \tau_{yz}^y}{\partial t} + (\Omega_y + \eta_S)\tau_{yz}^y = \mu \frac{\partial v_z}{\partial y} \tag{28}$$

$$\alpha_z \frac{\partial \tau_{yz}^z}{\partial t} + (\Omega_z + \eta_S)\tau_{yz}^z = \mu \frac{\partial v_y}{\partial z} \tag{29}$$

$$\alpha_x \frac{\partial \tau_{zx}^x}{\partial t} + (\Omega_x + \eta_S)\tau_{zx}^x = \mu \frac{\partial v_z}{\partial x} \tag{30}$$

$$\alpha_z \frac{\partial \tau_{zx}^z}{\partial t} + (\Omega_z + \eta_S)\tau_{zx}^z = \mu \frac{\partial v_x}{\partial z} \tag{31}$$

Finally, the 9 physical components are the sum of each splitted component:

$$v_\xi = v_\xi^\xi + v_\xi^\psi + v_\xi^\zeta \tag{32}$$

$$\tau_{\xi\xi} = \tau_{\xi\xi}^\xi + \tau_{\xi\xi}^\psi + \tau_{\xi\xi}^\zeta \tag{33}$$

$$\tau_{\xi\psi} = \tau_{\xi\psi}^\xi + \tau_{\xi\psi}^\psi \tag{34}$$

where ($\xi, \psi, \zeta = x, y, z$). As an example, the FDTD discretization for the splitted equation (8) leads to:

$$\begin{aligned} &\alpha_{x\left(i+\frac{1}{2},j,k\right)} \frac{v_x^{x\,n+\frac{1}{2}}\left(i+\frac{1}{2},j,k\right) - v_x^{x\,n-\frac{1}{2}}\left(i+\frac{1}{2},j,k\right)}{\Delta t} + \ldots \\ &\Omega_{x\left(i+\frac{1}{2},j,k\right)} \frac{v_x^{\,n-\frac{1}{2}}\left(i+\frac{1}{2},j,k\right) + v_x^{\,n+\frac{1}{2}}\left(i+\frac{1}{2},j,k\right)}{2} = \ldots \\ &-\frac{1}{\rho}\frac{\tau_{xx(i+1,j,k)}^n - \tau_{xx\,(i,j,k)}^{nn}}{\Delta x} \end{aligned} \tag{35}$$

And the update equation for this unknown is:

$$v_x^{x\,n+\frac{1}{2}}\left(i+\frac{1}{2},j,k\right) = C_1 v_x^{x\,n-\frac{1}{2}}\left(i+\frac{1}{2},j,k\right) - C_2\left(\tau_{xx(i+1,j,k)}^n - \tau_{xx\,(i,j,k)}^{nn}\right)$$

where constants matrix coeficients C_1 and C_2 are:

$$C_1 = \left(\frac{1 - \frac{\omega_{x\left(i+\frac{1}{2},j,k\right)}\Delta t}{2\alpha_{x\left(i+\frac{1}{2},j,k\right)}}}{1 + \frac{\omega_{x\left(i+\frac{1}{2},j,k\right)}\Delta t}{2\alpha_{x\left(i+\frac{1}{2},j,k\right)}}}\right) \qquad C_2 = \left(\frac{\frac{\Delta t}{\alpha_{x\left(i+\frac{1}{2},j,k\right)}\Delta x \rho}}{1 + \frac{\omega_{x\left(i+\frac{1}{2},j,k\right)}\Delta t}{2\alpha_{x\left(i+\frac{1}{2},j,k\right)}}}\right)$$

This discretization is applied for each of the 24 equations of the set (8-31).